Microsc. Microanal. Page 1 of 10
doi:10.1017/S1431927611000602

Microscopy AND Microanalysis

An Examination of Kernite ($Na_2B_4O_6(OH)_2 \cdot 3H_2O$) Using X-Ray and Electron Spectroscopies: Quantitative Microanalysis of a Hydrated Low-Z Mineral

Douglas C. Meier,[1,*] Jeffrey M. Davis,[1] and Edward P. Vicenzi[2,1]

[1]*Surface and Microanalysis Science Division, National Institute of Standards and Technology (NIST), 100 Bureau Dr. MS8371, Gaithersburg, MD 20899-8371, USA*
[2]*Museum Conservation Institute, Smithsonian Institution, 4210 Silver Hill Road, Suitland, MD 20746, USA*

Abstract: Mineral borates, the primary industrial source of boron, are found in a large variety of compositions. One such source, kernite ($Na_2B_4O_6(OH)_2 \cdot 3H_2O$), offers an array of challenges for traditional electron-probe microanalysis (EPMA)—it is hygroscopic, an electrical insulator, composed entirely of light elements, and sensitive to both low pressures and the electron beam. However, the approximate stoichiometric composition of kernite can be analyzed with careful preparation, proper selection of reference materials, and attention to the details of quantification procedures, including correction for the time dependency of the sodium X-ray signal. Moreover, a reasonable estimation of the mineral's water content can also be made by comparing the measured oxygen to the calculated stoichiometric oxygen content. X-ray diffraction, variable-pressure electron imaging, and visual inspection elucidate the structural consequences of high vacuum treatment of kernite, while Auger electron spectroscopy and X-ray photoelectron spectroscopy confirm electron beam-driven migration of sodium and oxygen out of the near-surface region (sampling depth ≈ 2 nm). These surface effects are insufficiently large to significantly affect the EPMA results (sampling depth ≈ 400 nm at 5 keV).

Key words: borate, kernite, hydrate, light elements, electron-probe microanalysis (EPMA), wavelength-dispersive X-ray spectroscopy (WDS), X-ray diffraction (XRD), X-ray photoelectron spectroscopy (XPS), variable-pressure scanning electron microscopy (VP-SEM), auger electron spectroscopy (AES)

Introduction

High-accuracy measurement of light elements is a challenge for electron-probe microanalysis (EPMA). The combination of low X-ray emission probabilities for elements with atomic numbers 4 (beryllium) through 11 (sodium) with high absorption cross sections for their characteristic X-rays (Goldstein et al., 2003) make quantification challenging. Despite these analytical difficulties, the broad academic interest in and the numerous industrial uses for materials rich in light elements spur the analyst to develop the best possible analytical methods for low-Z elements and to understand more precisely their measurement limitations.

Boron and borates in particular are of interest due to their many industrial applications, such as electroplating, radiation shielding, high-temperature glasses, dopants for silicon devices, agricultural products, and detergents (Sallay, 1980; Garrett, 1998), as well as the on-going research in topics such as glass nanoparticles (C&E News, 2008) and boron-induced superconductivity in semiconductors (Kreiner et al., 2008). Many electron microscopes use a thermionic electron source that features a lanthanum hexaboride (LaB_6) crystal emitter (Goldstein et al., 2003). Additionally, due to both the high water solubility of many of its common natural compounds and the fact that its isotopic ratio is a strong function of its environment of origin, boron serves as a tracer in near-surface earth science applications (Senior & Sloto, 2006). The importance of boron cluster chemistry is widely recognized; the 2009 recipient of the Priestley Medal, M. Frederick Hawthorne, is a noted pioneer in the field (Ritter, 2009).

The mineral kernite ($Na_2B_4O_6(OH)_2 \cdot 3H_2O$), which is a primary industrial source of boron and borates, is an example of a material for which electron-probe measurements should be particularly arduous. Kernite (named for a large ore deposit in Kern County, CA, USA) is one of a handful of naturally occurring inorganic materials that is made up exclusively of light elements ($Z \leq 11$), so its constituents feature low X-ray cross sections and high mass absorption effects. Specifically, boron's fluorescence yield is roughly 0.05% (Fig. 1) (Goldstein et al., 2003; Tanaka et al., 2008), and the mass absorption coefficients (MACs) for its K-L2,L3 X-ray line at 183 eV are over 15,000 in oxygen and 40,000 in sodium (Goldstein et al., 2003). This extremely fissile mineral cleaves readily on two crystal planes (Giese, 1966) and is highly soluble in water. It slowly absorbs water vapor from the atmosphere to eventually form natural borax ($Na_2B_4O_7 \cdot 10H_2O$) (Garrett, 1998) but is also known to lose structural water under vacuum conditions (Sennova et al.,

NIST Disclaimer: The full description of the procedures used in this article requires the identification of certain commercial products and their suppliers. The inclusion of such information should in no way be construed as indicating that such products or suppliers are endorsed by NIST or are recommended by NIST or that they are necessarily the best materials, instruments, software, or suppliers for the purposes described.

Received December 3, 2010; accepted April 14, 2011
*Corresponding author. E-mail: dmeier@nist.gov

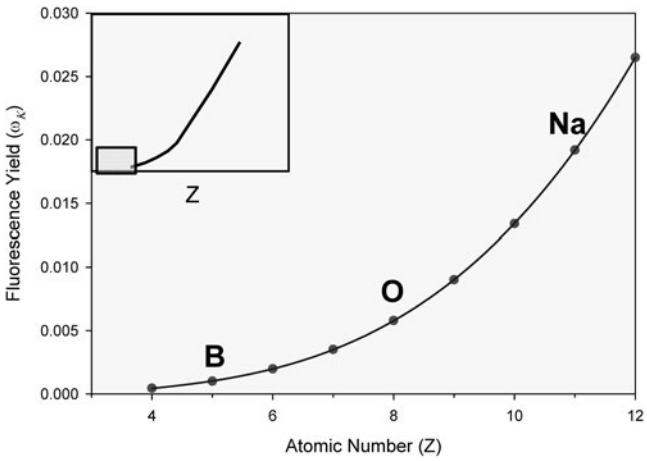

Figure 1. Fluorescence yields of the low-Z elements in kernite, adapted from Goldstein et al. (2003) and Tanaka et al. (2008).

2005). Thus, improper handling of kernite specimens could result in measurements either too low or too high in water content. Kernite is additionally electrically nonconductive, so issues of specimen charging and electron-beam-stimulated decomposition must be considered. However, since this readily friable hygroscopic hydrate occurs as large, high-purity single crystals (frequently exceeding 10 cm^3 at the Kern County deposit) of known composition (Rickwood, 1981) and structure (Giese, 1966), kernite offers an opportunity to rigorously develop analytical methods for other materials with similar challenges.

A primary goal of this study is to improve the accuracy and precision of boron quantification, as it is not only a high-value element for the above-mentioned applications, its concentration is also highly variable in modern materials such as semiconductors, glass, or steel (Jiménez et al., 1995; Garrett, 1998; May & Spanos, 2006) and in minerals (Hawthorne et al., 1996; McGee & Anovitz, 1996; Garrett, 1998). While EPMA results for kernite are reported in at least two other studies (Coppens et al., 1972; Cooper et al., 1973), neither energy dispersive X-ray spectroscopy (EDS) nor wavelength dispersive X-ray spectroscopy (WDS) spectra were published, and there is no indication that these data were used for quantitative analysis; rather, the method was employed as an impurity analysis. A comprehensive boron and boride WDS study (Bastin & Heijligers, 2000) presented methods of improving quantitative analysis of boron, notably through the use of peak area integration and area-to-peak factors as a means of obviating peak shift and shape errors; however, these methods were not demonstrated on delicate borates. Quantitative EDS methods have been demonstrated recently for MgB_2 (Birajdar et al., 2008); while it shares boron's analytical challenges with respect to mass absorption effects and low fluorescence cross section, it does not suffer the other material characteristic and experimental difficulties (resistivity; electron beam, water, and vacuum sensitivity) shared by the mineral borate hydrates. Wet chemical analysis, mass spectrometry, and vibrational spectroscopies are still the primary methods of identification and quantification of boron in minerals (Anovitz & Grew, 1996); however, EPMA of certain boron-bearing minerals, such as tourmalines and vesuvianite, has been performed successfully (McGee & Anovitz, 1996). The approach chosen in this study was to use a suite of surface science and electron probe techniques to quantify the composition of kernite and to monitor the deviations from bulk composition, if any, that occur during the measurement. In so doing, improved methods for microanalysis of light-element specimens and effective strategies for mitigating the pitfalls associated with measuring vacuum sensitive, beam sensitive, insulating, hydrated, and hygroscopic specimens will be realized. Furthermore, the suite of techniques used in this work provides a useful comparison of bulk/near surface (photons out) versus surface (electrons out) analysis techniques for this class of materials.

Materials and Methods

A kernite sample was obtained from the U.S. Borax Mine (operated by Rio Tinto Minerals) in Boron, CA, USA. The mineral was readily cleaved to prepare multiple fresh specimen surfaces for analysis. Specimens were then imaged by variable-pressure scanning electron microscopy (VP-SEM) using an FEI Quanta 200 F (FEI Company, Hillsboro, OR, USA) equipped with an EDAX 30 mm^2 Si(Li) energy dispersive spectrometer (EDAX, Mahwah, NJ, USA) for qualitative compositional analysis. A JEOL JXA-8600 electron microprobe (JEOL USA, Peabody, MA) equipped with LDEB [a layered diffracting element constructed of Mo/B_4C with an effective two-dimensional (2D) spacing of ≈20 nm], LDE1 (Si/W with an effective 2D spacing of ≈6 nm), and thallium acid phthalate (with a 2D spacing of 2.8 nm) diffracting crystals was used for EPMA-WDS. Data collection and analysis were performed using the Probe for EPMA (Probe Software, Inc., Eugene, OR, USA) software package, including real time correction for time-dependent effects and estimation of hydrogen. WDS measurements were repeated three times for area/peak factor calculations (Bastin & Heijligers, 2000) and ten times for time-dependent intensity (TDI) analysis of conventional peak-intensity data.

For the EPMA-WDS portion of the study, material standards of albite (sodium and oxygen) and cubic boron nitride (boron) were chosen. Due to the hygroscopicity and high solubility of kernite, any specimen preparation is required to be completely waterless to prevent sample transformation. While mounting the kernite specimens in a waterless methacrylate resin was successful, dry methods for polishing the mounts were inadequate owing to its friability. Attempts to polish using alcohol as the lapping fluid were also made, with similar deleterious effects on the specimen as those caused by water. Though imperfect, the cleavage faces of the mineral were deemed to be sufficiently flat over areas large enough for microanalysis. Freshly cleaved kernite specimens and the polished materials standards were carbon-coated simultaneously while mounted equidistant from the carbon source to reduce measurement errors in the compo-

sitional analysis owing to variability in the thickness of the carbon coating—an increasing concern as the analyzed X-ray lines approach lower voltages and thus encounter more acute mass absorption effects (the boron *K* X-ray MAC in carbon is nearly 6,000, while that of the oxygen *K* X-ray in carbon is over 11,000) in addition to beam deceleration effects (and therefore changes to E_0) encountered within the carbon film. Although coating with a thin noble metal film (e.g., 2 nm Pt or Au) is an alternative approach to preparing light-element specimens for analysis, the X-ray MACs for B K in Pt and Au exceed 10,800—greater than the carbon MAC, thus at least partially offsetting the benefits of thinner conductive metal films. Furthermore, since Auger electron spectroscopy (AES) was planned for these specimens, carbon was chosen over Pt or Au to avoid spectral overlaps with boron. Finally, a number of the standards that were analyzed were part of a multicomponent standards block, and it was determined that the possibility of contamination of the standard specimens with other metals posed too great a risk. Samples were cleaved, carbon-coated, and analyzed immediately after evacuation of the analysis chamber to reduce the impact of vacuum dehydration on the kernite specimen.

Surface deviations from bulk stoichiometry were determined using surface-sensitive AES and X-ray photoelectron spectroscopy (XPS). AES and XPS measurements were performed using a JEOL JAMP-7830F scanning Auger electron microprobe (JEOL USA) equipped with a concentric hemispherical energy analyzer, nonmonochromated Mg and Al X-ray sources, and an argon-ion sputter gun capable of either specimen surface cleaning or defocused ion flooding at low accelerating voltages for specimen charge neutralization. Electron spectra were collected on carbon-coated cleaved specimens and on uncoated specimens prepared by attaching 300 μm Cu grid apertures (ISO/TR 22335:2007) to mitigate spectroscopic artifacts due to specimen charging. The analysis areas of all of the specimens were cleaned by argon-ion beam prior to analysis; the carbon-coated samples had patches roughly 20 μm wide milled through the carbon so that the surface conductive pathway could be left as undisturbed as possible. The measurements were performed at 3.5 keV beam voltage and 1.5 nA beam current.

In the course of these studies, it became apparent that kernite was susceptible to both vacuum damage (Sennova et al., 2005) and electron-beam damage, complicating the analysis. To better understand the nature of the structural and compositional changes occurring under analysis conditions, X-ray diffraction (XRD) measurements were collected on untreated powdered kernite specimens, vacuum-treated (10^{-8} Pa for over 48 h) powdered specimens, and electron-beam (5 keV) irradiated powders using a Bruker AXS D8 (Bruker AXS, Ewing, NJ, USA) equipped with a Cu X-ray source. All analyses and treatments were performed on mixtures of kernite and LaB_6 powders at ambient temperature. LaB_6 was selected as an internal standard reference material (SRM) (SRM 660b, 2010) because its diffraction peaks are sharp, its pattern is well-characterized, its peaks do not overlap significantly with those of kernite, and it did not appear to undergo chemical reactions with sodium borate hydrates. Other candidates, such as aluminum oxide, were rejected; roughly one-third of the trace on the Na_2O-B_2O_3-Al_2O_3 phase diagram consistent with pure mixtures of kernite and alumina lies in the region assigned to sodium aluminoborate glass compositions (Züchner et al., 1998). The kernite-LaB_6 powder mixture was prepared for analysis by pressing it into tin foil.

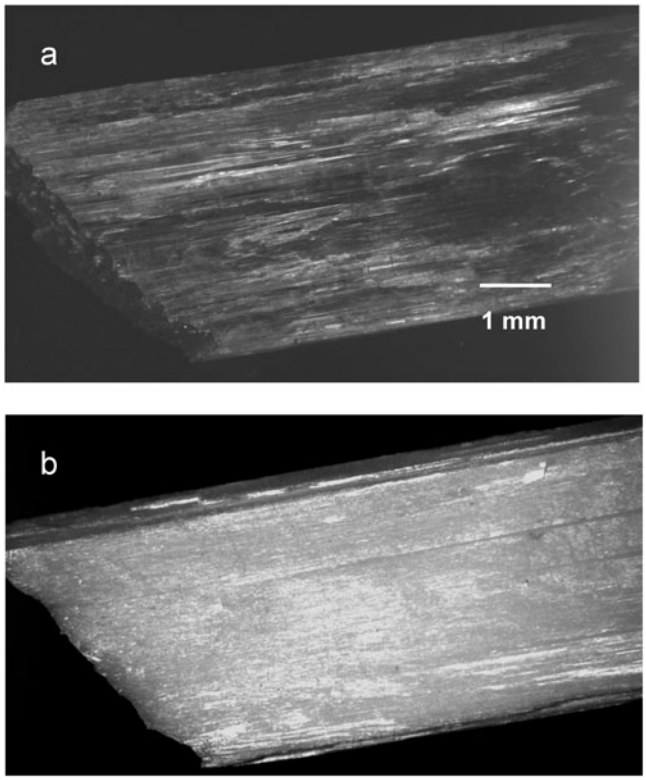

Figure 2. Photographic images of kernite (**a**) before and (**b**) after vacuum exposure.

Results and Discussion

Morphology and Thermodynamic Stability

Kernite is a transparent mineral that turns opaque white and becomes structurally weakened and crumbly after 24 h under ultrahigh vacuum (UHV) conditions (Fig. 2). This change in physical appearance is likely nonreversible, as the original clarity of the crystal did not return after re-exposure to ambient conditions for several months. The readily identifiable crystal structure of the mineral is rendered nearly amorphous by vacuum treatment with or without electron-beam irradiation (Fig. 3). Only a few weakly expressed low-angle diffraction peaks are still faintly distinguishable, and these are shifted to slightly higher angle (and thus smaller atomic-plane spacing) than the apparently analogous features in the as-received specimen. Although previous authors noted the appearance of an intermediate, "phase-I" (Sennova et al., 2005), under pressures lower than atmospheric, no such structure was observed in our mea-

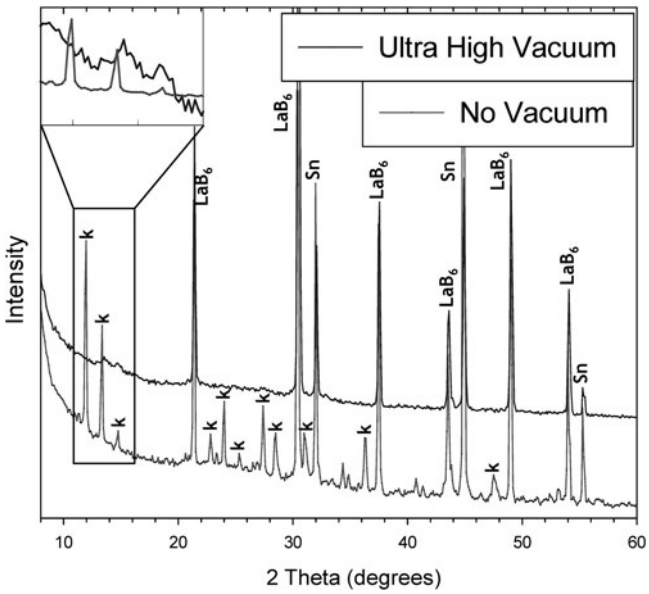

Figure 3. XRD spectra of the kernite—LaB_6 powder mixture before and after vacuum treatment (k = kernite). UHV conditions eliminate almost all long-range order in the kernite. Spectra collected after electron-beam irradiation and storage at ambient conditions post-vacuum treatment are indistinguishable from the spectra collected from the vacuum-treated specimen.

surements. One difference in specimen conditions between the two studies is the orders-of-magnitude lower pressures used in the present work relative to those described in Sennova et al. (2005). Following vacuum exposure and XRD analysis, the treated specimen was stored for 6 months at 30% RH and 25°C, after which additional XRD spectra were collected. The diffraction pattern of the vacuum-altered specimen did not change after this duration suggesting that the structural changes due to dehydration are irreversible, at least on the time scale of months.

Scanning electron microscope (SEM) imaging of macroscopic pieces of the mineral provided additional information regarding the nature of the phase transformation caused by exposure to vacuum conditions. The VP-SEM acquired at 5 keV with water vapor as the chamber atmosphere (1.1×10^2 Pa) can be used to eliminate charging problems observed during imaging of uncoated electrically-insulating specimens, such as kernite. A submicrometer film of a distinctly different phase is observed to have formed on the surface of crystal growth faces (Figs. 4, 5); however, the exposed underlying crystal appears to be largely intact. Since the XPS and AES spectra are collected under UHV conditions, initial SEM imaging was conducted to qualitatively assess the specimen damage and alteration. Carbon-coated and apertured (ISO/TR 22335:2007; Baer et al., 2010) macroscopic specimens both caused a substantial pressure increase when introduced into the UHV surface analysis chamber (from $<1\times10^{-7}$ Pa to $>4\times10^{-6}$ Pa); the friable, columnar, colorless mineral undergoes an accelerated efflorescence that transforms it into an extremely fragile opaque-white material. Both prepared specimens

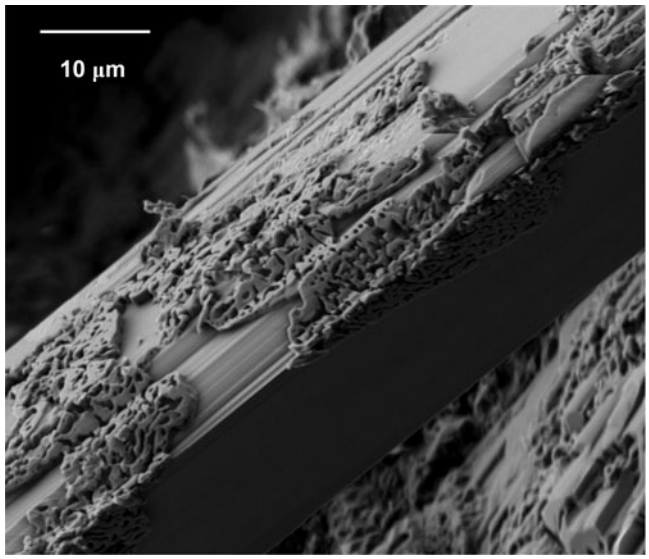

Figure 4. A gaseous secondary electron image of an as-received kernite crystal partially coated with an apparently amorphous submicrometer thick film (5 keV, $P_{H_2O} = 1.1 \times 10^2$ Pa).

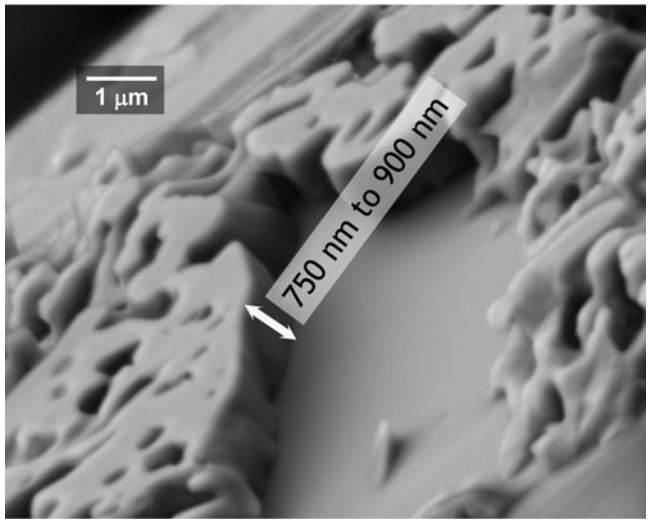

Figure 5. Magnified view of the native film formed on kernite in the VP-SEM (gaseous secondary electron).

yielded stable images in the Auger microprobe instrument (Fig. 6). The apertured specimen (Fig. 6a) suffered more total damage than the carbon-coated specimen, as evidenced by the greater degree of specimen cracking and roughening at 390 μm horizontal field width, 5 keV, and 10 nA (5.6×10^2 W/m^2). However, carbon-coating mitigates the most obvious beam damage and vacuum damage somewhat, maintaining a reasonably smooth cleavage face while imaging at 79 μm horizontal field width, 3.5 keV, and 1.5 nA (1.5×10^3 W/m^2) (Fig. 6b).

Compositional Analysis by EPMA

EPMA analysis was performed on a freshly cleaved surface using a defocused beam of 50 μm and a probe current of 61 nA. Preliminary EDS analysis of the material determined

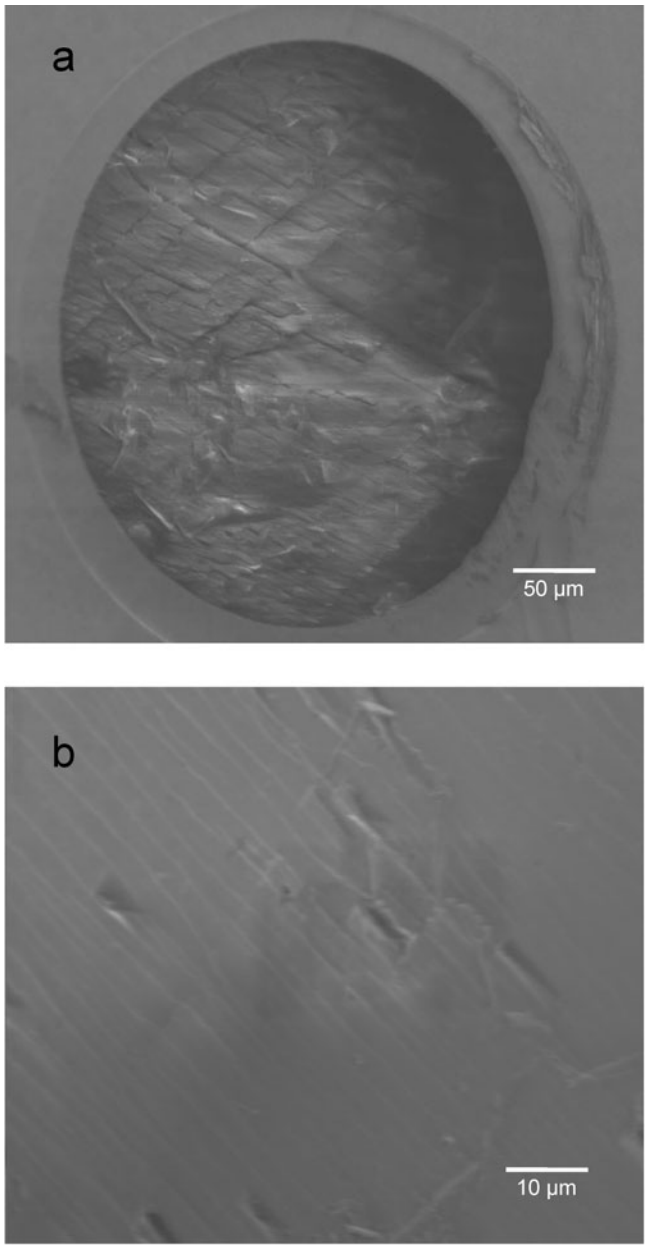

Figure 6. a: Secondary electron image of kernite as viewed under UHV conditions through a 300 μm copper aperture (390 μm horizontal field width, 5 keV, 10 nA). Fracturing of surface is noticeable. **b:** SEM image of carbon-coated kernite viewed under UHV conditions (79 μm horizontal field width, 3.5 keV, 1.5 nA). Surface fracturing is minimal; the hole milled into the carbon coating by the argon-ion beam is barely noticeable in the image.

that the greatest count rate in the $B_{K\text{-}L2,L3}$ peak (185 eV) was achieved at 5 keV. This finding was confirmed using the Mo/B_4C monochromator once the WDS system was fully calibrated. Although a 5 keV electron beam used for microanalysis may be regarded as a relatively low energy, the overvoltage (E_0/E_c) for $B_{K\text{-}L2,L3}$ is larger than the rule-of-thumb value of between 2 and 3. X-ray scattering at the interfaces of the layers in the large-effective-2D-spacing Mo/B_4C monochromator broadens the $B_{K\text{-}L2,L3}$ peak considerably, relative to the higher spectral resolution obtained in

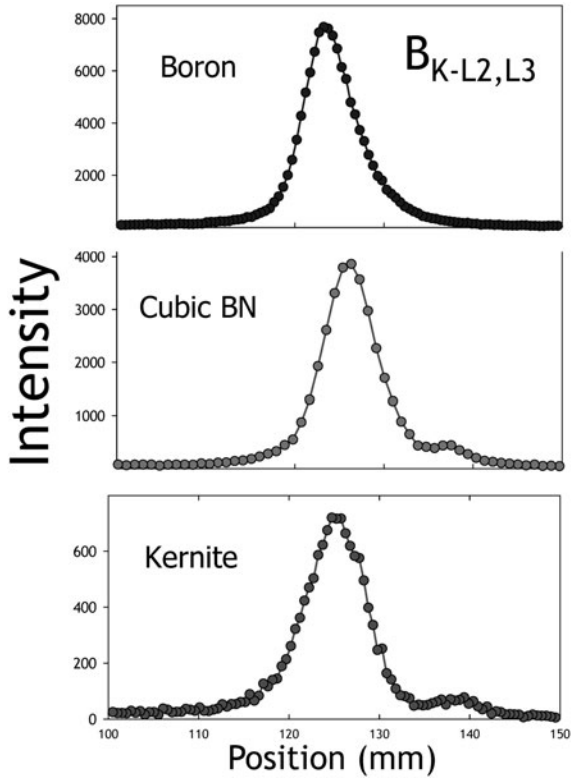

Figure 7. EPMA WDS wave scans of boron *K* for boron, boron nitride, and kernite measured (B_4C/Mo diffractor) under an electron probe at 5 keV beam energy, 61 nA beam current, and 50 μm beam spot.

an earlier quantitative EPMA boron study that employed lead stearate monochromators (Bastin & Heijligers, 2000). Despite poorer spectral resolution, a measureable peak shift and shape variation can be distinguished between boron metal, boron nitride, and kernite (Fig. 7).

Two approaches were employed in collecting boron EPMA measurements—(1) the area/peak factor method, which involves performing wavelength scans and integrating counts under the $B_{K\text{-}L2,L3}$ peak (Bastin & Heijligers, 2000), and (2) the conventional peak-intensity method, where high and low background intensities and a single boron peak intensity are measured (where peak shifts between the standard and borate are accounted for). For Method 1, the area/peak factor was determined for boron standards and kernite to derive accurate K-ratios. Nonlinear background fitting of the continuum obtained from the boron wavelength scans was used, providing a modest improvement over linear approximation. Method 1 results are extremely sodium deficient and somewhat boron deficient relative to the computed concentrations for stoichiometric kernite assuming no water present in the structure (Table 1). Method 2 results are less sodium deficient, but more boron deficient, than the Method 1 results.

Migration of sodium cations under the electron beam produces a change in the sodium X-ray signal as a function of time over successive measurements and is a well-documented problem for EPMA (e.g., Gedeon et al., 2000).

Table 1. Quantitative EPMA Results for Kernite.*

	Calculated Stoichiometric Atomic Mass % Kernite at Different Levels of Hydration			Area/Peak Factor Method		Peak Intensity Method, Time-Dependent Intensity (TDI)			
Element	Fully Hydrated Tetrahydrate ($Na_2B_4O_{11}H_8$)	Monohydrate ($Na_2B_4O_8H_2$)	Anhydrous ($Na_2B_4O_7$)	Atomic Mass %	RSD (%) ($n = 3$)	No H, No TDI Extrapolation	Include H, No TDI Extrapolation	Include H, Perform TDI Extrapolation	RSD (%) ($n = 10$)
Na	16.82	20.97	22.85	5.45	0.11	11.44	12.32	16.53	4.1
B	15.82	19.72	21.49	17.94	0.71	13.12	13.37	14.52	2.4
O	64.40	58.38	55.66	59.50	13.26	60.02	62.49	62.49	1.3
H_{calc}	2.95	0.92	0.00	—	—	—	3.88	3.09	3.1
Total	100	100	100	82.88		84.57	94.29	96.63	

*Mean composition of kernite as determined by EPMA-WDS using area/peak factors (Bastin & Heijligers, 2000) and conventional peak intensity analysis (Pouchou & Pichoir, 1984), assuming no hydrogen, including hydrogen in the analysis, and correcting for time dependency of the X-ray signal. These are compared to the stoichiometric compositions of kernite (Garrett, 1998) and sodium borates with fewer waters of hydration. Because of the decreased electron beam dose, the peak intensity method produced the more accurate Na quantitative values; therefore, only those data are used to estimate the effects of both TDI and H. The algorithm patterned after Pouchou and Pichoir (1984) gave the highest consistent analytical totals, so it was used throughout the experiment to correct for matrix effects.

This issue is particularly acute for sodium-rich materials because sodium migration beyond the ≈400 nm sampling depth [as estimated by CASINO v.2.42 (Drouin et al., 2007)] will greatly alter the measured intensity and therefore skew the results not only for sodium but also for other elements that sodium impacts in the matrix correction, e.g., by absorption. To account for this time-dependent intensity (TDI) the signal was subsampled throughout the measurement, a nonlinear regression was used to fit the results, and the fitted curve was extrapolated back to zero time to estimate the initial sodium X-ray intensity (Fig. 8). For these experiments, TDI corrections were employed to adjust for significant sodium loss and modest boron gain, while oxygen values were unchanged during the course of the measurements. Finally, although hydrogen cannot be analyzed by EPMA, its concentration can be estimated indirectly by comparing the measured oxygen value to the oxygen computed by stoichiometry of substituent binary oxides (Nash, 1992; Donovan & Vicenzi, 2008). Since the measured oxygen value exceeds that for the sum of oxygen in the binary oxides (Na_2O and B_2O_3), one can assign the "excess" oxygen to water, compute the concentration of hydrogen in a hydrated material, and finally reperform the matrix correction for the analysis. When one accounts for the effects of sodium time dependency and makes an estimate for the amount of water, the EPMA results closely resemble those of fully hydrated kernite (Table 1).

The greatest absolute difference between the fully corrected Method 2 results and those of fully hydrated kernite is the 2% mass fraction oxygen deficit, which can be attributed in part to rapid water loss due to electron-beam heating on a time scale shorter than measurement subsampling. This effect is consistent with the evolution of vapor noted in the reflected light image of the sample surface immediately after the electron beam was unblanked and began irradiating the sample. The near-instantaneous water loss also accounts for the mass fraction sum being less than 100%. The investigated sample from the U.S. Borax mine is quite homogeneous, as indicated by the small relative standard deviations (Table 1).

Surface Compositional Analysis

The AES spectra of both the carbon-coated specimen and the specimen with an affixed copper grid aperture were severely affected by charging; flooding the analysis area during the measurement with a defocused 300 V argon-ion beam at 100 nA reduced the local surface charging sufficiently to collect usable Auger spectra for both specimen preparations (Fig. 9). The spectra collected from the apertured specimen suffer smaller charging effects than those from the carbon-coated specimen, but a small copper signal (probably from redeposition of material sputtered from the grid aperture by the neutralizing argon ion flood) obscures the spectral region where the sodium signal is expected. The carbon-coated specimen does not have this problem, so its spectra are unambiguously devoid of sodium peaks; however, the boron and oxygen peaks are

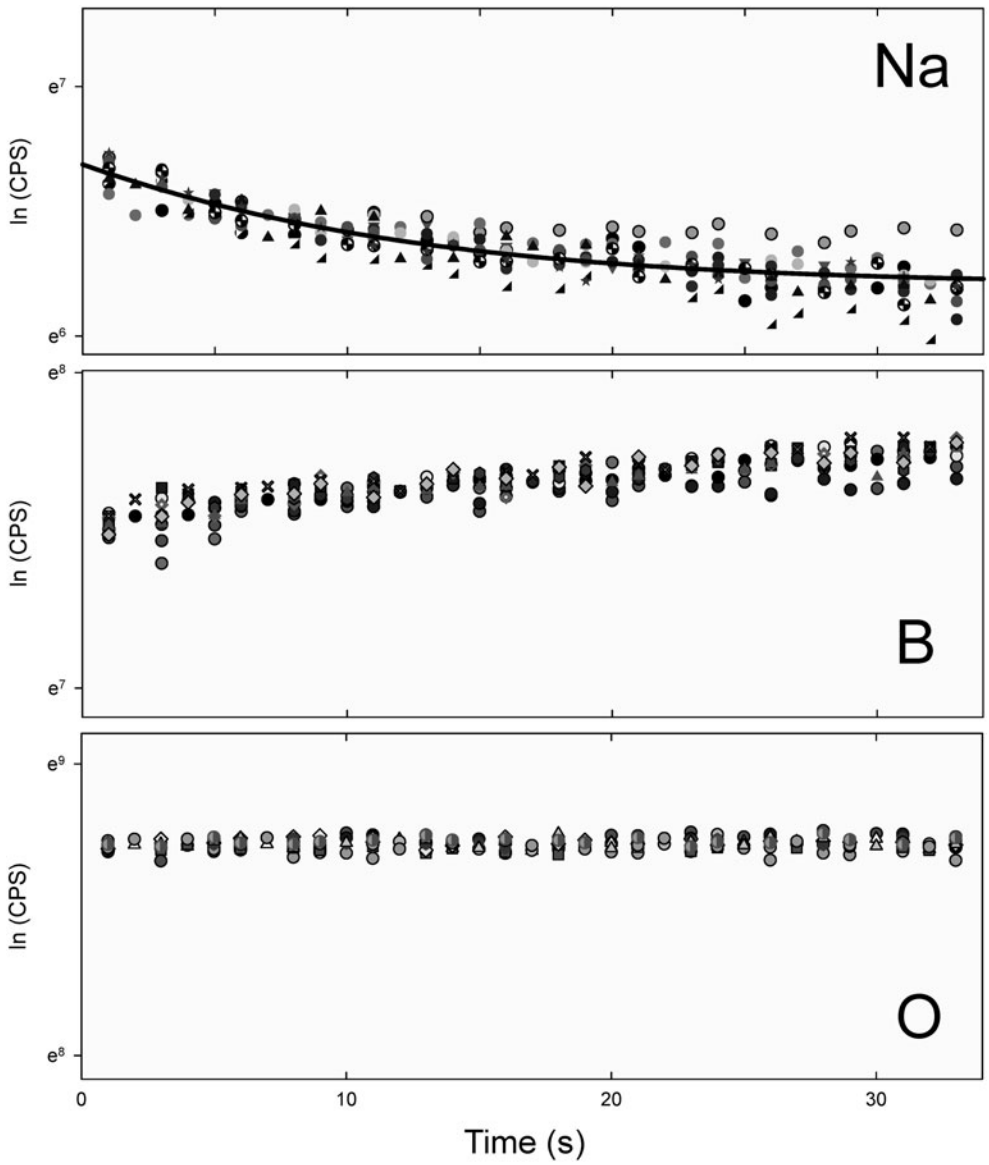

Figure 8. EPMA time series of the sodium, boron, and oxygen peak maxima in kernite ($n = 10$). As the sodium signal decreases (mean value as solid black line) markedly, the boron signal increases slightly, while that of oxygen remains constant. All measurements are included to show measurement uncertainty.

both shifted and skewed to lower energy. Furthermore, the intensity of the secondary electron background is significantly lower than is otherwise expected for Auger spectra below 100 eV. Together, these two effects suggest a slightly positive charging of the carbon-coated specimen with respect to the apertured specimen. Using the method of relative sensitivity factors applied to peak intensities to calculate atomic fraction (Davis et al., 1976), it was determined that the boron:oxygen ratio is roughly 3:2 within the sampled volume, compared to 4:11 in kernite and 4:7 in fully dehydrated kernite—indicating a considerable loss of surface oxygen, deficient for even an anhydrous borate.

While the Auger measurement shows that the near-surface region of the kernite is both sodium- and oxygen-deficient under long-term electron-beam irradiation, it does not establish whether this modification is due in greater part to the electron beam or to vacuum decomposition. XPS (Al *K* nonmonochromated) was performed on the specimens to provide qualitative information on the composition at approximately the same depth (≈2 nm) as that probed by AES, but to do so without electron-beam excitation. The XPS results (Fig. 10) show considerable sodium intensity in the near-surface region, indicating that the reduction of sodium concentration there is induced predominantly by the electron beam.

Conclusions

Despite the challenges, it was possible to measure the composition of (largely) undamaged kernite using electron-probe techniques. Vacuum exposure results in efflorescence,

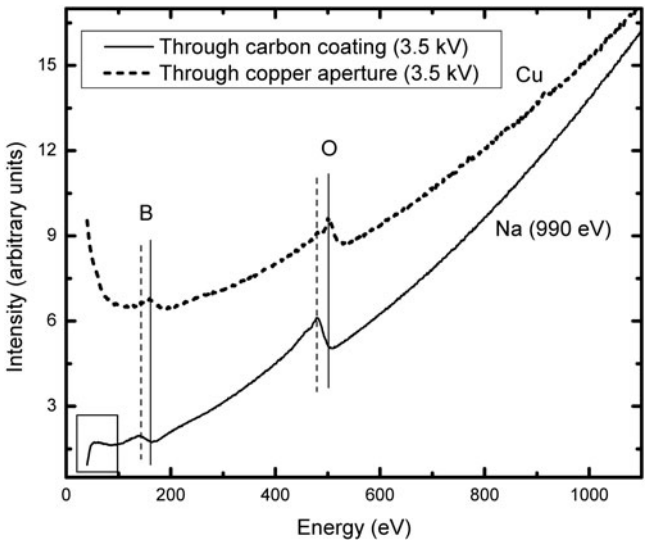

Figure 9. Auger electron spectra of kernite with affixed aperture (dashed) and with carbon coating (solid). Vertical lines situated on the peaks of the spectra highlight the energy offset due to specimen charging differences between the carbon-coated and the through-aperture specimen. The low-energy intensity loss in the carbon-coated specimen (box) indicates more significant positive charging effects than experienced by the apertured specimen. Sodium features are not visible in either spectra, though it is possible that the copper features present in the spectra of the apertured specimen obscure trace sodium.

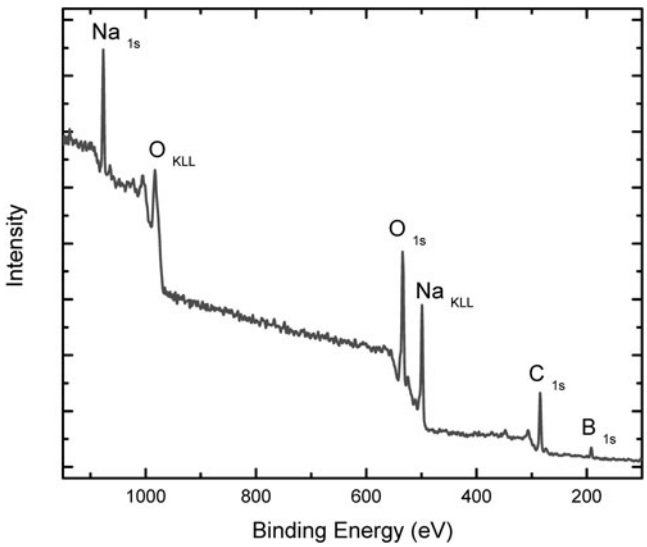

Figure 10. XPS spectrum of kernite (nonmonochromated Al *K* radiated). Features for sodium, boron, oxygen, and carbon are present. The discrepancy between the sodium feature's prominence in XPS and its absence in AES indicates electron-beam-induced migration.

while electron-beam irradiation results in sodium migration out of the surface region, lattice-bound water loss, and perhaps oxygen loss from the borate chains, all likely causes of deviation of the analysis from the stoichiometric composition. Uncertainties in the boron measurement could be due in part to the choice of standards (boron nitride is not a borate, and the peak shapes, while similar, are not equivalent) as well as the decomposition of the material under analysis conditions. Correcting for electron-beam-exposure time is critical for obtaining a high-quality compositional measurement and for mitigating sodium-loss measurement uncertainties. However, there is likely an instantaneous water loss upon electron-beam exposure that cannot be accounted for, nor measured by, current WDS technology in a TDI study using these instruments. The XRD results suggest that exposure to protracted low pressures nearly eliminates the long-range order in the material. The data collected here, taken together, suggest a transformation under analysis in which the water is largely stripped from the crystal surface, while sodium and oxygen defects produced by the beam over time shatter the long-range order (Fig. 11). Nevertheless, the measured values obtained by prompt EPMA of cleaved surfaces are close estimates of not only the three elements that can be measured directly using these techniques, but also enable good estimation of the hydrogen in the specimen. This specimen is quite pure, and no contaminants other than carbon were identified within the limits of detection for any of the spectroscopies utilized.

Proper specimen preparation is critical to successfully performing these measurements. Polishing fails due to differences in hardness between the kernite, the resin, and the material standards, as well as water sensitivity. Simultaneous carbon coating of specimens and standards was necessary to eliminate errors due to signal absorption in the coating. Minimizing the length of time under vacuum and backward extrapolation with respect to time provided the best results for EPMA, but for AES these strategies are not practical—the amount of time required for recovery of UHV conditions after introducing the specimen to the chamber preclude meaningful TDI data in AES.

Given the difficulties and uncertainties of the measurement, the task of distinguishing hydrated borates from each other is nontrivial; therefore, EPMA compositional analysis is currently an inadequate approach for confirming the discovery of a new borate hydrate mineral. However, extraction of semiquantitative information is possible. Furthermore, the time-dependent data provide clues as to the nature of the electron-beam damage suffered by kernite during analysis, specifically that the loss in sodium and water from the analysis zone results in lower mass absorp-

Table 2. Mass Absorption Coefficients (MACs) for Selected Low-Z Elements.*

	Emitter		
Absorber	Na	B	O
Na	574.4	**40,649**	**3,513**
B	1,154	2,861	**7,754**
O	**4,084**	**15,774**	1,181
H	6.2	**1,723**	60.7

*MACs for each source and absorber present in kernite (Goldstein et al., 2003).

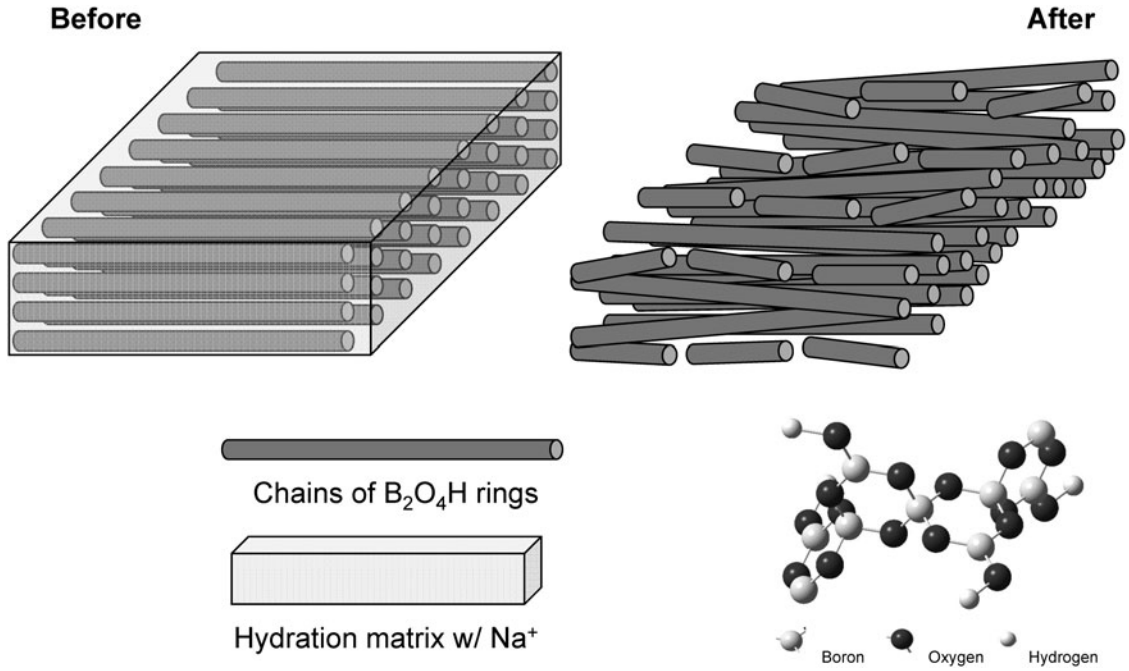

Figure 11. Schematic representation of the effects of vacuum conditions on kernite. As the hydration matrix is removed, the stacked infinite chains of $(B_2O_4H)_x$ collapse, eliminating the long-range structure of the mineral.

tion of boron and oxygen X-rays. As sodium and water leave the analysis area, mass absorption of boron X-rays decreases, contributing to the increase in signal observed in the time series plot (Fig. 8). The likelihood that this signal change is due to migration of boron into the analysis zone is low because it is the strongest absorber for oxygen *K* (Table 2), yet the oxygen time series does not show a signal decrease, even though AES confirms its surface concentration is reduced by the electron beam. While oxygen is also leaving the analysis zone, loss of sodium reduces the oxygen *K* absorption, and so the time-dependent intensity is constant. Therefore, as the sodium signal (and concentration) drops during electron beam analysis, the boron signal increases while the oxygen remains constant because the expected signal increase caused by diminishing sodium mass absorption effects is canceled by the loss of oxygen due to electron-beam damage.

Acknowledgments

The authors acknowledge Scott Wight for assistance with VP-SEM. The authors thank Jeffrey Stultz and Alex Davidson of Rio Tinto Minerals for providing the kernite specimens and for helpful discussions.

References

Anovitz, L.M. & Grew, E.S. (1996). Mineralogy, petrology, and geochemistry of boron: An introduction. In *Boron: Mineralogy, Petrology, and Geochemistry*, Grew, E.S. & Anovitz, L.M. (Eds.), pp. 1–40. Washington, DC: Mineralogical Society of America.

Baer, D.R., Lea, A.S., Geller, J.D., Hammond, J.S., Kover, L., Powell, C.J., Seah, M.P., Suzuki, M., Watts, J.F. & Wolstenholme, J. (2010). Approaches to analyzing insulators with Auger electron spectroscopy: Update and overview. *J Electron Spectrosc Related Phenomena* **176**, 80–94.

Bastin, G.F. & Heijligers, H.J.M. (2000). Quantitative electron probe microanalysis of boron. *J Solid State Chem* **154**, 177–187.

Birajdar, B., Peranio, N. & Eibl, O. (2008). Quantitative electron microscopy and spectroscopy of MgB_2 wires and tapes. *Superconductor Sci Technol* **21**, 073001.

C&E News. (2008). Making borosilicate nanoparticles is now possible. *Chem Eng News* **86**, 34–35.

Cooper, W.F., Larsen, F.K., Coppens, P. & Giese, R.F. (1973). Electron population analysis of accurate diffraction data. V. Structure and one-center charge refinement of the light-atom mineral kernite, $Na_2B_4O_6(OH)_2 \cdot 3H_2O$. *Am Mineral* **58**, 21–31.

Coppens, P., Cooper, W.F. & Larsen, F.K. (1972). Charge-distribution in light-atom mineral kernite. *Science* **176**, 165–166.

Davis, L.E., MacDonald, N.C., Palmberg, P.W., Riach, G.E. & Weber, R.E. (1976). *Handbook of Auger Electron Spectroscopy*. Eden Prairie, MN: Physical Electronics Division, Perkin-Elmer Corporation.

Donovan, J.J. & Vicenzi, E.P. (2008). Water by EPMA—New Developments. *Microsc Microanal* **14**(S2), 1274–1275 (CD-ROM).

Drouin, D., Couture, A.R., Joly, D., Tastet, X., Aimez, V. & Gauvin, R. (2007). CASINO V2.42—A fast and easy-to-use modeling tool for scanning electron microscopy and microanalysis users. *Scanning* **29**, 92–101.

Garrett, D.E. (1998). *Borates: Handbook of Deposits, Processing, Properties, and Use*. San Diego, CA: Academic Press.

Gedeon, O., Hulinsky, V. & Jurek, K. (2000). Microanalysis of glass-containing alkali ions. *Microchimica Acta* **132**, 505–510.

Giese, R.F., Jr. (1966). Crystal structure of kernite, $Na_2B_4O_6(OH)_2 \cdot 3H_2O$. *Science* **154**, 1453–1454.

Goldstein, J.I., Lyman, C.E., Newbury, D.E., Lifshin, E., Echlin, P., Sawyer, L., Joy, D.C. & Michael, J.R. (2003). *Scanning*

Electron Microscopy and X-Ray Microanalysis. New York: Springer Science and Business Media.

Hawthorne, F.C., Burns, P.C. & Grice, J.D. (1996). The crystal chemistry of boron. In *Boron: Mineralogy, Petrology, and Geochemistry*, Grew, E.S. & Anovitz, L.M. (Eds.), pp. 41–115. Washington, DC: Mineralogical Society of America.

ISO/TR 22335:2007. (2007). Surface chemical analysis—Depth profiling—Measurement of sputtering rate: Mesh-replica method using a mechanical stylus profilometer. Geneva, Switzerland: International Organization for Standardization.

Jiménez, J.A., González-Doncel, G. & Ruano, O.A. (1995). Mechanical properties of ultrahigh boron steels. *Adv Mater* **7**, 130–136.

Kreiner, M., Muranaka, T., Kato, J., Ren, Z.-A., Akimatsu, J. & Maeno, Y. (2008). Superconductivity in heavily boron-doped silicon carbide. *Sci Technol Adv Mater* **9**, 044205.

May, G.S. & Spanos, C.J. (2006). *Fundamentals of Semiconductor Manufacturing and Process Control*. Hoboken, NJ: John Wiley & Sons, Inc.

McGee, J.J. & Anovitz, L.M. (1996). Electron probe microanalysis of geologic materials for boron. In *Boron: Mineralogy, Petrology, and Geochemistry*, Grew, E.S. & Anovitz, L.M. (Eds.), pp. 771–788. Washington, DC: Mineralogical Society of America.

Nash, W.P. (1992). Analysis of oxygen with the electron microprobe: Applications to hydrated glass and minerals. *Am Mineral* **77**, 453–457.

Pouchou, J.-L. & Pichoir, R. (1984). Un nouveau modèle de calcul pour la microanalyse quantitative par spectrométrie de rayons X—Partie I: Application à l'analyse d'échantillons homogènes. *La Récherche Aerospatiale* **3**, 167–192.

Rickwood, P.C. (1981). The largest crystals. *Am Mineral* **66**, 885–907.

Ritter, S.K. (2009). Boron dreams: Priestley medalist M. Frederick Hawthorne has some unfinished business. *Chem Eng News* **87**, 12–14.

Sallay, S.I. (1980). Process for producing boron compounds from borate ores. United States Patent #4196177.

Senior, L.A. & Sloto, R.A. (2006). Arsenic, boron, and fluoride in ground water in and near diabase intrusions, Newark Basin, southeastern Pennsylvania. USGS Scientific Investigations Report 2006-5261. Reston, VA: U.S. Geological Survey.

Sennova, N.A., Bobnova, R.S., Filatov, S.K., Paufler, P., Meyer, D.C., Levin, A.A. & Polyakova, I.G. (2005). Room, low, and high temperature dehydration and phase transitions of kernite in vacuum and in air. *Cryst Res Technol* **40**, 563–572.

SRM 660b. (2010). NIST SRM 660b—Line position and line shape, standard for powder diffraction. Gaithersburg, MD: National Institute of Standards and Technology.

Tanaka, M., Takeguchi, M. & Furaya, K. (2008). X-ray analysis and mapping by wavelength dispersive X-ray spectroscopy in an electron microscope. *Ultramicroscopy* **108**, 1427–1431.

Züchner, L., Chan, J.C.C., Müller-Warmuth, W. & Eckert, H. (1998). Short-range order and site connectivities in sodium aluminoborate glasses: I. Quantification of local environments by high-resolution ^{11}B, ^{23}Na, and ^{27}Al solid-state NMR. *J Phys Chem B* **102**, 4495–4506.